Clinical Cancer Research

Impact of Blood–Brain Barrier Integrity on Tumor Growth and Therapy Response in Brain Metastases

Matthias Osswald[1,2], Jonas Blaes[1,2], Yunxiang Liao[1,2], Gergely Solecki[1,2], Miriam Gömmel[1,2], Anna S. Berghoff[1,2], Laurent Salphati[3], Jeffrey J. Wallin[4], Heidi S. Phillips[4], Wolfgang Wick[1,2], and Frank Winkler[1,2]

Abstract

Purpose: The role of blood–brain barrier (BBB) integrity for brain tumor biology and therapy is a matter of debate.

Experimental Design: We developed a new experimental approach using *in vivo* two-photon imaging of mouse brain metastases originating from a melanoma cell line to investigate the growth kinetics of individual tumor cells in response to systemic delivery of two PI3K/mTOR inhibitors over time, and to study the impact of microregional vascular permeability. The two drugs are closely related but differ regarding a minor chemical modification that greatly increases brain penetration of one drug.

Results: Both inhibitors demonstrated a comparable inhibition of downstream targets and melanoma growth *in vitro*. *In vivo*, increased BBB permeability to sodium fluorescein was associated with accelerated growth of individual brain metastases. Melanoma metastases with permeable microvessels responded similarly to equivalent doses of both inhibitors. In contrast, metastases with an intact BBB showed an exclusive response to the brain-penetrating inhibitor. The latter was true for macro- and micrometastases, and even single dormant melanoma cells. Nuclear morphology changes and single-cell regression patterns implied that both inhibitors, if extravasated, target not only perivascular melanoma cells but also those distant to blood vessels.

Conclusions: Our study provides the first direct evidence that nonpermeable brain micro- and macrometastases can effectively be targeted by a drug designed to cross the BBB. Small-molecule inhibitors with these optimized properties are promising agents in preventing or treating brain metastases in patients. *Clin Cancer Res; 22(24); 6078–87. ©2016 AACR.*

See related commentary by Steeg et al., p. 5953

Introduction

Brain metastases are the most frequent malignant intracranial tumors in adults, and a devastating complication of solid cancers, severely affecting survival and quality of life of patients. Melanomas have a particularly high propensity to spread to the brain, as about 50% of patients with metastasized (stage IV) melanoma suffer from brain metastases at the time of death (1). The incidence of brain metastases seems to be rising, partly due to the fact that some novel compounds that can control tumor growth outside the central nervous system (CNS) do not, or only partially, penetrate the blood–brain barrier (BBB), as suggested for trastuzumab in HER2-positive breast cancer (2). Therefore, tumor cells that have successfully invaded the brain may not be affected by these therapeutic agents, making the brain a potential "sanctuary site" for cancers (3).

There is an ongoing controversy about the role of BBB breakdown in affecting the activity of systemic therapies against brain metastases (4–6). To make the issue even more complicated, a considerable heterogeneity of therapeutically relevant BBB breakdown seems to exist: In an experimental brain metastases model of breast cancer, the majority of lesions showed an at least partial compromise of the blood–tumor barrier, but only approximately 10% showed an uptake of chemotherapy in cytotoxic concentrations (7). A highly variable uptake of classical and targeted therapeutic agents was also found in resected brain metastases from patients (8). In health but also in most CNS diseases, the different components of the BBB hinder the vast majority of therapeutic agents to access the brain, which includes endothelial cells, tight junctions, the basement membrane, pericytes, and astrocytic end feet and efflux transporters [e.g., glycoprotein P (P-gp) and other multidrug-resistance proteins, and breast cancer resistance protein (BCRP; or ABCG2)] that regulate the extravasation of xenobiotics (9, 10). Several techniques have been tested to direct therapeutic agents across the BBB, including disruption of the BBB, modification of drugs, inhibition of efflux transport, and "Trojan horse" approaches that use endogenous transporter properties of the BBB (9).

Thus, the BBB might hinder brain penetration of promising novel therapeutic agents, which includes inhibitors of the PI3K–

[1]Neurology Clinic and National Center for Tumor Diseases, University Hospital Heidelberg, Heidelberg, Germany. [2]Clinical Cooperation Unit Neurooncology, German Cancer Consortium (DKTK), German Cancer Research Center (DKFZ), Heidelberg, Germany. [3]Department of Drug Metabolism and Pharmacokinetics, Genentech, Inc., South San Francisco, California. [4]Department of Cancer Signaling and Translational Oncology, Genentech, Inc., South San Francisco, California.

Note: Supplementary data for this article are available at Clinical Cancer Research Online (http://clincancerres.aacrjournals.org/).

Corresponding Author: Frank Winkler, Neurology Clinic and National Center for Tumor Diseases, University Hospital Heidelberg, Im Neuenheimer Feld 400, Heidelberg D-69120, Germany. Phone: +4962-2156-7107; Fax: +4962-2156-7554; E-mail: frank.winkler@med.uni-heidelberg.de

doi: 10.1158/1078-0432.CCR-16-1327

Translational Relevance

It remains a matter of dispute whether the blood–brain barrier (BBB) is relevant for treatment of brain tumors with systemic therapies and at which stages. Here, we show that corecording of the dynamic brain metastatic process in a mouse model, and the regional BBB integrity in these metastases, can provide valuable information in this respect. Metastases residing behind an intact regional BBB can effectively be targeted with a PI3K/mTOR inhibitor that has been modified to increase its brain penetration, whereas the nonmodified-related PI3K/mTOR inhibitor only has effects on metastases with a disturbed BBB. The results of this study have implications for future development of drugs aiming at improved therapeutic efficacy in neuro-oncology. They are also informative for the development of preventive strategies using systemic drugs for those patients who are at risk of developing brain metastases but without detectable, permeable macrometastases yet.

Akt–mTOR (PAM) pathway (11, 12). The PAM pathway plays a role in cell survival, growth, proliferation, and invasion in many human cancers, at least under certain circumstances (11). Recent evidence suggests that both PI3K and mTOR complex 1 (mTORC1) need to be targeted in parallel to exert maximum effectivity and to overcome resistance (13).

Here, we investigated the potential of the PI3K/mTOR inhibitor GNE-317 to affect melanoma brain metastases of different stages, depending on microregional BBB breakdown. GNE-317, which has not entered clinical development, is a potent dual PI3K/mTOR inhibitor (inhibiting both mTORC1 and mTORC2) that was rationally designed to bypass the two main exclusion transporters constituting the BBB (P-gp and BCRP) and has already shown effects in preclinical mouse glioma models (14, 15). GDC-0980, a closely related dual PI3K/mTOR inhibitor but a substrate of P-gp and BCRP (16), was used as a control drug to understand how the BBB affects antitumor activity of small-molecule inhibitors not optimized for BBB penetration.

Materials and Methods

Cell line

A melanoma cell line was chosen because these tumor entities do not show angiogenic growth during earlier stages in brain metastases (17). Angiogenesis with disruption of the BBB would have influenced the bioavailability of an applied drug, and, thus, could have interfered with the results of this study. A2058 melanoma cells (obtained from the ATCC-CRL-11147, 07/2011) were kept under standard media conditions (DMEM, 10% FBS, P/S); no further authentication of the cell line had been done, but they were regularly checked for *Mycoplasma* infections by PCR. A2058 cells were lentivirally transduced with a cytoplasmic RFP [tdTomato, LeGo-T2 vector, kind gift from A. Trumpp, German Cancer Research Center (DKFZ)] and a nuclear GFP [pLKO.1-LV-GFP, Addgene #25999, Elaine Fuchs (Howard Hughes Medical Institute and The Rockefeller University)], as described previously (18), to illustrate the shape of the metastasizing cells (cytoplasmic signal) and to allow an exact quantification of nuclei (nuclear signal). To increase the capability to form brain metastases after cardiac injection, three brain passages of these cells were performed before the trial commenced (brains of mice were removed 4 weeks after intracardiac injection of $A2058^{RFP/H2B\text{-}GFP}$ cells and dissociated, and tumor cells were expanded *in vitro* and reinjected). *In vitro* growth was similar to the nontransfected and non–brain-seeking parental cells. Furthermore, although having a higher overall propensity to form brain metastases due to higher efficacy to master all steps of the metastatic cascade, the single steps of this brain metastatic cascade did not change during *in vivo* growth.

Compounds and *in vitro* studies

GNE-317 [5-(6-(3-methoxyoxetan-3-yl)-7-methyl-4-morpholinothieno[3,2-d]pyrimidin-2-yl)pyrimidin-2-amine] and GDC-0980 were synthesized by Genentech, Inc. For IC_{50} tests, cells were monitored in an xCELLigence Real-Time Cell Analyzer (RTCA) system (Roche Diagnostics). A2058 cells were seeded in quadruplets of 2,000 cells each in an RTCA E-plate and treated with different doses of GNE-317 or GDC-0980 (0.5, 2, 10, and 50 μmol/L) in 0.5% DMSO and culture media. Cells were observed for 143 hours after application of the compounds, and the maximum cell index during this time versus concentration was used for the dose–response curves. For description of the cell index, see ref. 19. Analysis was performed using the RTCA Software 1.2.1.1002 (ACEA Biosciences, Inc.).

For immunoblotting, A2058 cells were treated with GDC-0980, GNE-317, or vehicle at the indicated dose (10 μmol/L) for 3 or 6 hours, respectively. Preparation of cell lysates and immunoblot was performed as described previously (20). Membranes were incubated with polyclonal rabbit anti-phospho-NDRG1Thr346 (1:5,000; Cell Signaling Technology); goat anti-GAPDH (1:1,000; Linaris); rabbit anti-AKT (1:1,000; Cell Signaling Technology); goat anti-NDRG1 (1:2,500; Abcam); and PathScan Multiplex Cocktail I, consisting of Phospho-AKT (S473), Phospho-RPS6 Ser235/236, eIF4E, Phospho-p44/42 MAPK (Erk1/2) (Thr202/Tyr204), Phospho-p90RSK Ser380 (all rabbit; 1:200; Cell Signaling Technology) overnight at 4°C. Staining with secondary horseradish peroxidase–conjugated donkey anti-goat or anti-rabbit (1:5,000; GE Healthcare) was followed by immunodetection with ECL Plus Western Blotting Detection System (GE Healthcare).

Animals and animal procedures

Eight- to 10-week-old male NMRI-nu/nu mice (20 g, Charles River Germany) received a cranial window as described previously (21). For tumor cell injection, mice were anesthetized with ketamine/xylazine (100 mg/kg i.p. and 10 mg/kg i.p., respectively) and laid on their back, and their skin was disinfected. Tumor cells (1×10^6 in 0.1 mL) were then slowly injected into the left cardiac ventricle. Success of the heart injection was controlled by (i) retrograde blood flow into the syringe and (ii) postinterventional fluorescence control of the brain under a binocular equipped with a fluorescence set up (Nikon Intensilight C-HGFI). Only mice with visible tumor cells under the cover glass were used for further analysis.

For tumor treatment, mice received GNE-317 (25 mg/kg), GDC-0980 (7.5 mg/kg), or 0.5% methylcellulose/0.2% polysorbate (MCT, carrier substance) by oral gavage in a maximum volume of 0.2 mL every day. The two substances were dissolved in MCT directly before gavage. In preliminary pharmacokinetic studies, GDC-0980 administered at 1, 5, or 10 mg/kg presented exposure (AUC and C_{max}) that increased in a dose-proportional manner (Supplementary Fig. S1). On the basis of the exposure

obtained with GNE-317 at 25 mg/kg, the dose for GDC-0980 was adjusted to 7.5 mg/kg to achieve comparable predicted AUC (Supplementary Fig. S1; ref. 16). Mice were treated until a weight loss of 20% or until neurologic symptoms appeared. To reduce the possibility of initial spontaneous metastases regression, we waited with the start of treatment until at least brain micrometastases had formed. This was very heterogeneous between the animals and between different metastases in one animal. Six mice were treated in both treatment groups, and 4 mice in the MCT group. The number of metastases that were followed over time with *in vivo* two-photon microscopy was 19 (GNE-317), 15 (GDC-0980), and 11 (MCT). The mean treatment per metastasis was 6.68 days for the GNE-317 group and 6.33 days for the GDC-0980 group ($P = 0.406$; Kruskal–Wallis one-way ANOVA on ranks). After death, mice were routinely checked for systemic metastases, and advanced systemic disease was generally found. All animal procedures were performed in accordance with the institutional laboratory animal research guidelines after approval of the Regierungspräsidium Karlsruhe, Germany (governmental authority).

In vivo two-photon microscopy

For *in vivo* multiphoton laser-scanning microscopy (MPLSM), a ZEISS LSM 7MP equipped with a Coherent Chameleon Ultra II laser was used. Images were taken with a 20×/1.0 W-Plan-Apochromat objective (ZEISS). The signals of the used fluorophores were differentiated by different excitation wavelengths and different filters: FITC dextran (angiograms; 2M MW; FD-2000S; Sigma-Aldrich), sodium fluorescein (permeability scans; F6377; Sigma-Aldrich), and tdTomato (tumor cell cytoplasm) were excited at 750 nm, whereas GFP-labeled nuclei and TRITC dextran (angiograms; 500 kDa; 52194; Sigma-Aldrich) were excited at 850 nm. A BP500-550 filter was used for the green fluorophores, and a BP575-610 filter was used for the red fluorophores. Two independent images were acquired consecutively at 750 and 850 nm in two channels to allow an unambiguous detection of the fluorophores. Laser power was kept as low as possible, and before the permeability measurements, it was reduced to a minimum to avoid any laser-induced changes in BBB permeability. Standard gains were set between 700 and 750, and standard *z*-interval was 3 μm. Mice were fixed using a custom-build fixation system with a titan ring, and body temperature was kept constant by a heating-pad system. The painless fixation made it possible to use an isoflurane narcosis with a concentration of 1% to 2%. Mice were imaged maximum every 3 days during treatment. Only at the start of treatment, the permeability of the BBB was measured; at the other time points, only the cell number was determined. To relocate the same brain region and same tumor cells in repetitive measurements over time, both stereotactic coordinates of the microscope and the superficial blood vessel architecture (that normally does not change over time and, thus, provides a stable road map) were used.

Measurement of BBB integrity

Metastases were categorized into permeable versus nonpermeable metastases by intravenous injection of the low molecular sodium fluorescein (MW 376.27 g/mol/L; F-6377; Sigma-Aldrich) during the *in vivo* imaging procedure via a catheter system into the tail veins of the mice. Prior to this, a very small amount of high molecular dextran (which does not leak out of the vessels) had been injected to obtain angiograms for orientation.

(i) For the dynamic sodium fluorescein measurements, the sodium fluorescein signal inside the blood vessel and in the tumor was measured at the time of sodium fluorescein injection (different time points starting before, and over a maximum of 30 minutes after sodium fluorescein injection). The ratio of the sodium fluorescein signal in the tumor region (outside the blood vessel) divided by the sodium fluorescein signal inside the blood vessel was defined as the permeability index that was used for the correlation with the daily growth rates. For this analysis, a subpopulation of 23 metastases was analyzed, because multiple nonpermeable metastases in one mouse could only be analyzed within a limited time frame (approximately 1 hour) to avoid false categorization into the group of permeable metastases by sodium fluorescein diffusion in the brain; in 1 of 6 mice with permeable metastases, a second permeable metastasis could be measured as a second time point. For the permeability index, we chose a cutoff value of 0.4 to differentiate between permeable and nonpermeable metastases, because this best reflected the value where bona fide extravasation of sodium fluorescein (>0.4) versus no such extravasation (<0.4) could be detected by careful review of the images obtained.

(ii) To categorize multiple brain metastases in the same animal into permeable and nonpermeable ones at the start of treatment with GNE-317 or GDC-0980, the extravasation of sodium fluorescein after intravenous injection was measured (fluorescein signal/background signal at one time point). Importantly, for metastases which had been also measured with the dynamic method, there was a 100% consistency between both methods to define permeable versus nonpermeable metastases.

Image processing and quantifications

ZEISS ZEN software was used for image acquisition and primary image calculation. Then, the images were further analyzed using ImageJ software (NIH) for the analysis of sodium fluorescence intensity inside the tumor tissue and inside the blood vessel, or images were transferred to Imaris (Bitplane) to calculate and process 3D images. If necessary, changes in brightness, contrast, or color balance were made to whole images. In these 3D projections, cell numbers were calculated for each time point using the spot function of Imaris. Ratios were calculated for each metastasis, and daily growth rates were calculated. Micrometastases were defined as metastases with 3 to 50 cells, whereas metastases with >50 cells were called macrometastases. For a better description of the different growth patterns of permeable and nonpermeable metastases, we measured two diameters: the longest metastasis diameter ("length") and the longest diameter orthogonally to the first one ("width"). The ratio between these two diameters (width/length) would be near "1" for round metastasis and near "0" for a very thin and long metastasis. For analyses of treatment response, all metastases had been grouped in (i) permeable (=extravasation of SF, ball-like growth) or (ii) nonpermeable (=no extravasation of SF, co-optive growth) metastases. To assess whether cancer cells distant from brain microvessels can still be reached by the compounds, we measured the distance of a tumor cell apoptotic event to the nearest blood vessel and the distance of the tumor cell nucleus most distant from this blood vessel, but not nearer to another blood vessel. By dividing these two distances, the "blood vessel proximity index" for apoptotic events was

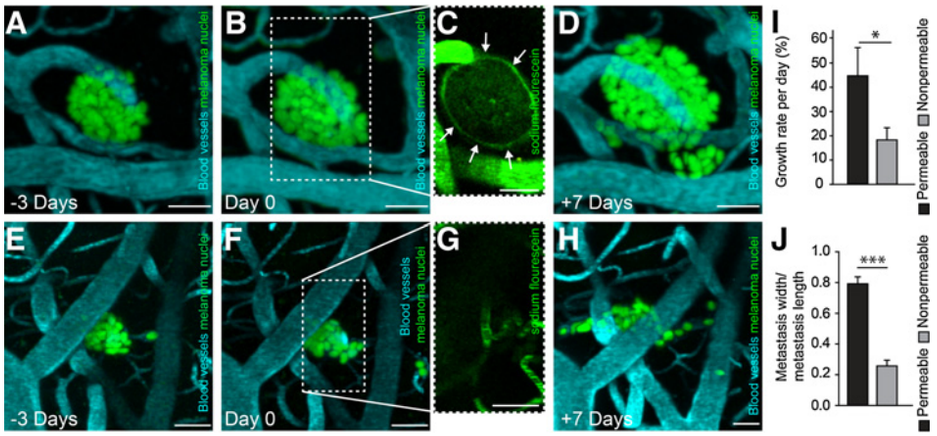

Figure 1.

Brain metastases with BBB breakdown grow faster than nonpermeable metastases. Representative growth of a permeable (**A–D**) and a nonpermeable (**E–H**) A2058 melanoma metastasis over 10 days in the live mouse brain (MCT control mice are shown, sham treatment started at day 0). **C** and **G** illustrate the permeability measurement with sodium fluorescein directly after intravenous injection (one focal plane only). In permeable metastasis, sodium fluorescein rapidly leaked out of the vessels (**C**, arrows: border of the metastasis), whereas in nonpermeable metastases, no sodium fluorescein signal appeared outside the blood vessel (**G**). Permeable metastases grew faster than nonpermeable metastasis (**I**, $n = 7$ permeable metastases from $n = 6$ animals; $n = 16$ nonpermeable metastases from $n = 12$ animals; *, $P = 0.018$; Mann–Whitney rank sum test). **J,** Different growth patterns of permeable and nonpermeable metastases. Nonpermeable metastases grew linear along preexisting brain microvessels (ratio near "0"), whereas the permeable metastases grew more ball like (ratio near "1") ($n = 7$ permeable metastases; $n = 16$ nonpermeable metastases; ***, $P < 0.001$; t test. **A–J,** All images were acquired by *in vivo* MPLSM; 3D reconstructions of z-stacks of 57–66 μm (**A, B,** and **D**) and 84–87 μm depth (**E, F,** and **H**); error bars show SE; scale bars, 30 μm.

calculated. That means, a blood vessel proximity index of 0.5 reflects an apoptotic event in a tumor cell in the middle of a blood vessel supply territory, of 0.0 reflects an apoptotic event in a tumor cell directly adjacent to a blood vessel, and of 1.0 reflects an apoptotic event in the tumor cell most distant to its nearest blood vessel. The mean values for groups represent the overall likelihood of apoptotic events in relation to the nearest perfused brain microvessel.

Statistical analysis

For statistical analysis of differences between treatment groups or permeability, SigmaPlot software (Systat Software, Inc.) was used. Normal distribution was tested by the Shapiro–Wilk test. For normally distributed data, a two-sided Student's t test or an ANOVA was used; otherwise a Mann–Whitney rank sum test or a Kruskal–Wallis one-way ANOVA on ranks was used. For the correlation between the daily growth rate and the permeability index, a linear regression was performed. Statistical significance was stated for P values < 0.05. The used tests are noted in the figure legends.

Results

BBB breakdown is associated with faster growth of individual brain metastases

First, we asked the principal question of whether BBB integrity and the speed of tumor growth are interrelated in individual brain metastasis. To optimally address this biologically important issue, and to later investigate differential drug effects, we established an animal model that combined *in vivo* multiphoton time-lapse imaging of growing hematogeneous melanoma brain metastases with corecording of microvascular permeability in the same metastasis. Tumor cells were injected intracardially and had to master all steps of the brain metastatic cascade (17) to grow to micrometastases (defined as 3–50 tumor cells) and, eventually, macrometastases (>50 tumor cells). BBB integrity was measured by extravasation of the fluorescent small-molecule sodium fluorescein (22), which has a molecular weight of 376, similar to that of GNE-317 (414), GDC-0980 (499), and most other small-molecule inhibitors in clinical use (which are typically below 500). To optimize morphologic information of melanoma cells and to enable automated counting of cells in individual metastases over time we stably transduced the cells with lentiviruses encoding both tdTomato (for cytoplasmic morphology) and H2B-GFP (for nuclear morphology).

First, we established a methodology that allowed us to distinguish two principal subgroups of melanoma brain metastases by their extravasation pattern of sodium fluorescein: metastases with versus without relevant BBB breakdown at this site (Supplementary Fig. S2A; for details, see Materials and Methods). Interestingly, the growth speed of A2058 melanoma brain metastases with BBB breakdown (permeable metastases; Fig. 1A–D) was higher than in metastases with an intact BBB (nonpermeable metastases; Fig. 1E–H and Supplementary Fig. S2B). Quantification of the growth of 23 single metastases over time confirmed that the average daily growth rates of permeable metastases exceeded that of nonpermeable metastases more than 2-fold (Fig. 1I). Nonpermeable metastases were more frequent (71.2% of all observed metastases) than permeable metastases at the time of investigation. The appearance of new blood vessels over time—that is, true angiogenesis—was observed in only one very large (>20,000 tumor cells) and permeable metastasis (Supplementary Fig. S2C). Of note, both metastases types (permeable and nonpermeable) had a distinct growth pattern: whereas metastases with a BBB breakdown were growing ball like and well demarcated toward the surrounding brain parenchyma, metastases with an intact BBB grew by

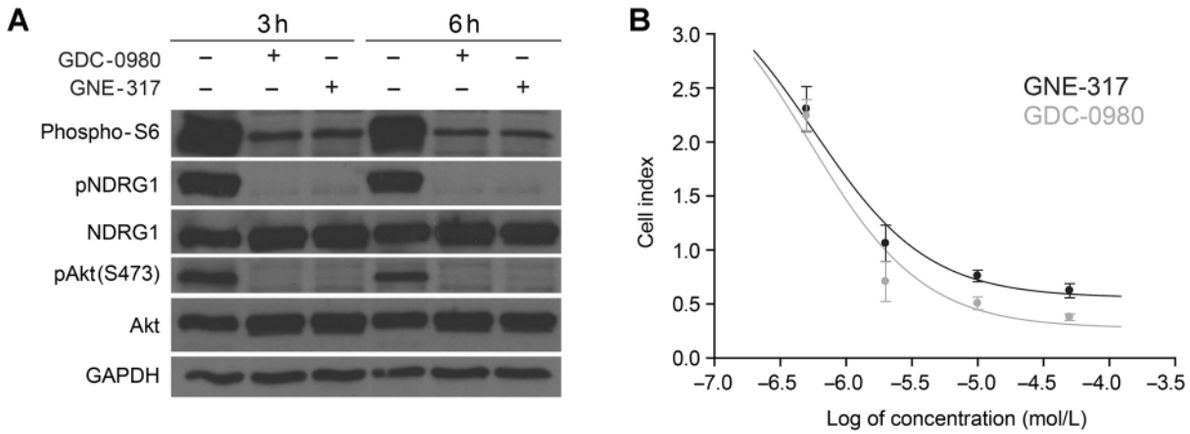

Figure 2.

GNE-317 and GDC-0980 are similarly effective *in vitro*. **A,** Western blot analysis showing similar inhibition of downstream targets of mTORC1 (pS6) and mTORC2 [pAkt(S473) and pNDRG1) for both GNE-317 and GDC-0980 in A2058 melanoma cells, whereas Akt and NDRG1 appear (compensatorily) upregulated. The compounds were used in a dose of 10 μmol/L. **B,** Dose–response curves for GNE-317 and GDC-0980; calculated IC_{50} from RTCA *in vitro* data were 0.57 μmol/L for GNE-317 and 0.53 μmol/L for GDC-0980.

co-option of preexisting cerebral microvessels in the brain (Fig. 1D vs. H; quantification, Fig. 1J).

GNE-317 and GDC-0980 similarly inhibit the mTOR pathway *in vitro*

Before conducting *in vivo* experiments, we first tested whether both compounds have a similar impact on the mTOR pathway in A2058 melanoma cells and cell proliferation and viability *in vitro*. For that purpose, we performed a Western blot analysis of the downstream targets of mTORC1 (pS6) and mTORC2 [pAkt(S473) and pNDRG1] to evaluate the inhibiting potential of the compounds used in melanoma cells *in vitro*. Treatment with identical doses of GNE-317 and GDC-0980 led to a strong inhibition of both complexes, as indicated by alteration of their downstream targets; importantly, there was no detectable difference between both compounds (Fig. 2A). Accordingly, we determined the *in vitro* IC_{50} of both compounds using an RTCA and found comparable results (0.53 μmol/L for GDC-0980 and 0.57 μmol/L for GNE-317; Fig. 2B). Finally, bioavailability studies of both compounds were performed in mice to adjust the daily dose of GNE-317 to that of GDC-0980 to achieve comparable drug exposure of brain metastases-bearing mice (Supplementary Fig. S1).

GNE-317, but not GDC-0980, targets both permeable and nonpermeable brain micro- and macrometastases

The major aim of this study was to investigate how permeability of an individual brain metastasis influences the therapeutic activity of the BBB-optimized (GNE-317) versus the original (GDC-0980) PI3K/mTOR inhibitor. The mean start of treatment was 19.3 days after tumor injection for the GNE-317 and the GDC-0980 groups, and 23.8 days after injection for the MCT control group ($P = 0.322$; ANOVA). The starting time point was chosen that late to minimize the possibility of spontaneous, not therapy-related, regression of brain micrometastases; in A2058 brain metastases, spontaneous regression has been shown to be a very rare event at this time point (17). Before start of treatment, the daily growth rate for all metastases was not significantly different across the 3 groups (22.07% for the GNE-317 group, 19.31% for the GDC-0980 group, and 16.82% for the MCT group; $P = 0.985$; Kruskal–Wallis one-way ANOVA on ranks), and, thus, metastases sizes did not differ significantly across the groups either (Supplementary Fig. S3A).

After classification into permeable and nonpermeable metastases (Supplementary Fig. S3B), treatments were initiated. The daily growth rate of permeable metastases was reduced with both compounds, leading to a comparable growth rate reduction (Fig. 3A–H). This confirmed that both compounds were indeed given in biologically equivalent, efficient doses. Importantly, only GNE-317 was able to significantly inhibit the growth of nonpermeable metastases, which was even associated with a moderate mean shrinkage of those metastases without a BBB breakdown (Fig. 3I–L). In contrast, GDC-0980 therapy had no significant effects on nonpermeable brain metastases (Fig. 3M–P). The therapeutic effect of GNE-317 stayed significant when analyzed separately for nonpermeable micro- versus macrometastases (Fig. 4A), but only micrometastases shrank, whereas macrometastases still grew. Control animals treated with the carrier solution alone (MCT control) did not show any differences in tumor growth rate over time (Fig. 1; Supplementary Fig. S3C).

In one mouse, we were lucky to detect the rare event of tumor cell dormancy: a brain microregion with four dormant A2058 melanoma cells could be followed until day 31, with typical slow movement of dormant melanoma cells in their perivascular niche (Fig. 4B and C; ref. 17). There were no signs of increased microvascular permeability in this brain region (data not shown). Of note, we never observed the death/disappearance of single dormant tumor cells more than 30 days after tumor cell injection (17). Hence, we initiated GNE-317 treatment in this animal at day 31 to investigate whether these dormant cancer cells can be targeted by the CNS-optimized small-molecule inhibitor. Indeed, the dormant cells died under treatment (Fig. 4D and E); at day 39, only cellular remnants of these cells could be detected (Fig. 4E).

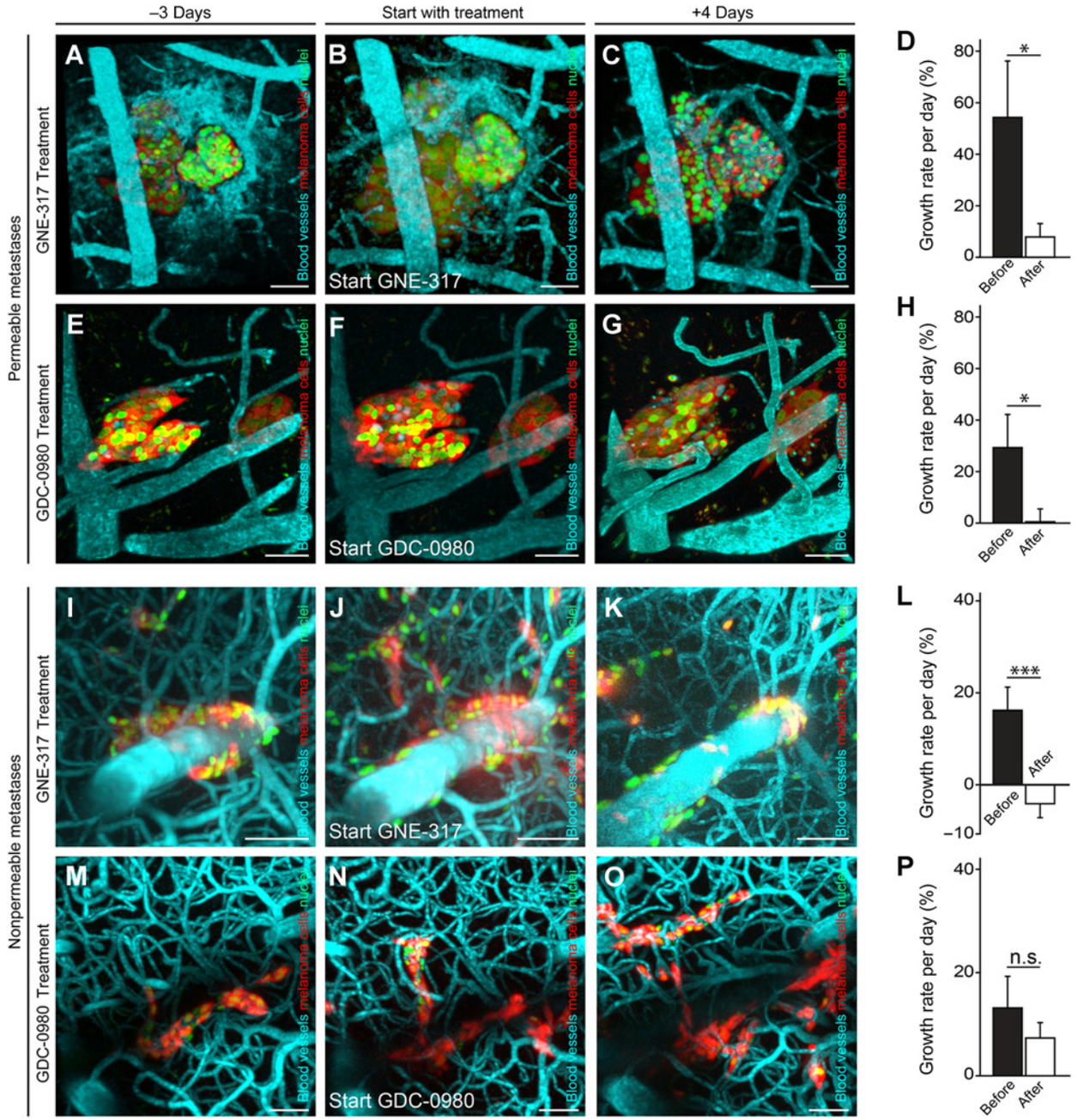

Figure 3.

GNE-317 targets both permeable and nonpermeable metastases. Permeable brain metastases that were treated with GNE-317 (**A–C**) showed a significant reduction in the daily growth rate after start of treatment (**D,** $n = 3$ metastases from $n = 3$ animals; *, $P = 0.0241$; two-sided t test), as well as permeable metastases that were treated with GDC-0980 (**E–G**; quantification **H**: $n = 6$ metastases from $n = 3$ animals; *, $P = 0.017$; Mann–Whitney rank sum test). Nonpermeable brain metastases that were treated with GNE-317 (**I–K**) responded with a significant reduction in their growth rate, even shrinkage (**L,** $n = 16$ metastases from $n = 6$ animals; ***, $P < 0.001$; Mann–Whitney rank sum test), whereas treatment with GDC-0980 (**M–O**) had no significant effect on their growth rate per day (**P,** $n = 9$ metastases from $n = 6$ animals; $P = 0.481$; Mann–Whitney rank sum test). All images were acquired by *in vivo* MPLSM; 3D reconstructions of z-stacks of 69–81 μm (**A-C**), 39–57 μm (**E–G**), 300–438 μm (**I–K**), and 207–210 μm depth (**M–O**); error bars show SE; scale bars, 50 μm.

Effects of mTOR/PI3K inhibition on nuclear morphology in melanoma cells *in vivo*

We finally used the opportunity of our new model to acquire images of melanoma cell nuclei under treatment to search for changes in nuclear morphology that are indicative of cellular apoptosis (23)—that is, condensation and fragmentation of nuclei. In MCT control animals, nuclear morphology was normal, and frequent mitoses were observed *in vivo* (Fig. 5A). No nuclear

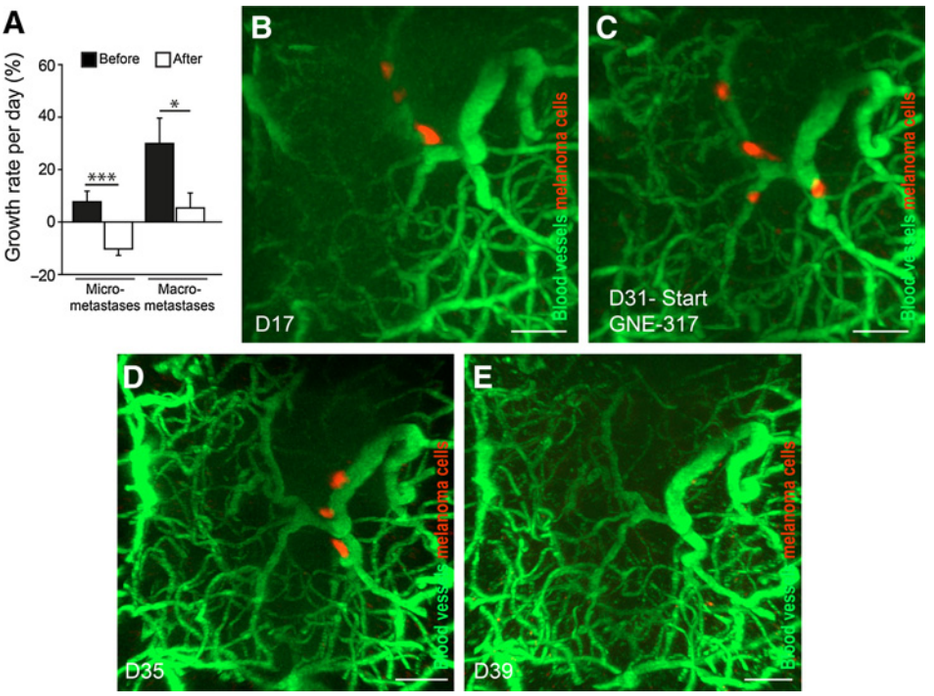

Figure 4.
GNE-317 targets micrometastases and dormant tumor cells. **A,** Subgroup analysis of GNE-317–treated metastases, separately for nonpermeable micro- ($n = 10$) and macrometastases ($n = 6$) (***, $P < 0.001$ and *, $P = 0.033$; two-sided t tests). **B–E**, Treatment response of single, long-term, nonproliferating and nonregressing, thus dormant, melanoma cells. The single cells are slowly moving during dormancy. After start of treatment with GNE-317 at D31 (**C**), the dormant cells regressed within 8 days (**E**). All images were acquired by *in vivo* MPLSM; 3D reconstructions of z-stacks of 156–192 μm depth (**B–E**); scale bars, 50 μm.

changes were detectable in nonpermeable metastases treated with GDC-0980 either (data not shown), in line with the lack of efficacy on metastasis outgrowth in this group. In contrast, permeable metastases treated with both inhibitors and nonpermeable metastases treated with GNE-317 showed striking pathologies of nuclear morphology (Fig. 5B–D). A deeper analysis revealed that the nuclear changes indicative of apoptosis were not restricted to tumor cells with direct contact to a cerebral microvessel. To the contrary, tumor cells distant from the nearest blood vessel (as determined in 3D-image stack analysis) showed even more apoptotic events than those cells that were found in the perivascular space, as indicated by a blood vessel proximity index of >0.5 for all three conditions (Fig. 5D).

Discussion

In this study, we aimed to investigate the impact of BBB integrity on the brain metastatic process, particularly the targetability of different stages of brain metastases with systemic drugs. Here, we show that a high heterogeneity in BBB disruption between individual metastatic lesions is present, and that this heterogeneity has a significant impact on the therapeutic efficacy of small-molecule inhibitors.

By using *in vivo* multiphoton imaging of the dynamic process of metastases formation in brain microregions, we first discovered that the integrity of the BBB was closely associated with how fast these individual metastases grew. It has been clear before that the majority of brain macrometastases—that is, metastases of more than a millimeter diameter, which are detectable with common imaging techniques in patients—show signs of some BBB breakdown, although to a different extent (7, 24–26). In our model, the BBB was either open or intact in the observed time frame, and we did not observe the transition of a nonpermeable metastasis into a permeable one or vice versa. The permeability-related characteristic growth patterns (growth by co-option of preexisting microvessels versus a ball-like growth, respectively) never changed over time. This dichotomy of either nonpermeable or permeable metastases made it possible to later study how the BBB affects drug activities. Whether metastases with a disrupted BBB grow faster than those with an intact BBB is due to either the better supply of nutrients or growth factors by BBB disruption or specific biological properties of the tumor cells remains an open question. In line with our observation, contrast-enhancing metastases had larger volumes than nonenhancing ones in an experimental model of breast cancer brain metastases (26), but there was no strong correlation between brain metastases size and permeability in five breast cancer mouse models at the time of death of the animal (27). In another study, brain metastases of different tumor entities (melanoma, breast, colon, renal carcinoma) showed no leakage of sodium fluorescein in early stages, and leakage was directly correlated with the size; here, two distinct growth patterns were observed also (28). For the first time, our study was able to determine the current growth speed of brain metastases on a microscopic level at the time of permeability measurement, and it supports the existence and biological relevance of a positive correlation of both.

Here, we report that therapy with a PI3K/mTOR inhibitor modified to optimally penetrate the BBB (GNE-317) leads to a response in all metastases (independent of BBB integrity), whereas treatment with the related but non-BBB–permeable agent GDC-0980 leads to a therapy response in permeable metastases only. Interestingly, the study also revealed that brain metastatic tumor cells in the perivascular space (niche) show less apoptotic events under PI3K/mTOR inhibition than those tumor cells that are farther away from the nearest blood vessel. This indicates two things: First, after successful extravasation of the compounds, no drug delivery problems seem to exist within a brain metastasis for the two PI3K/mTOR inhibitors tested, at least none of therapeutic

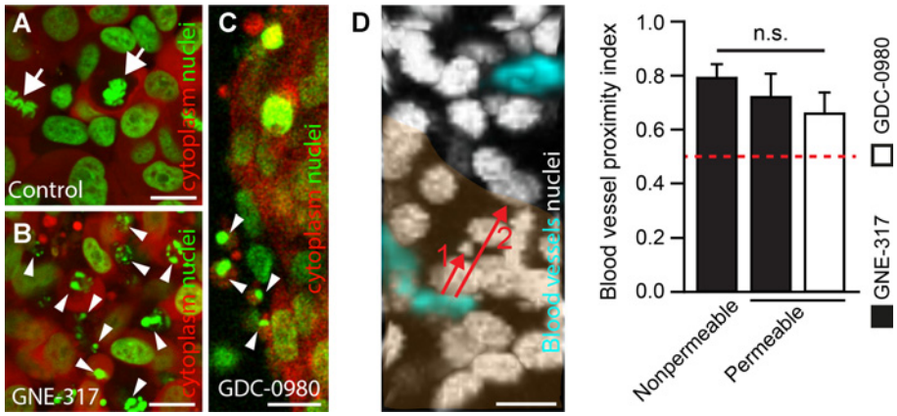

Figure 5.

Treatment-induced cellular damage is not restricted to the perivascular space. **A,** Nuclear morphology of A2058 melanoma cells that were treated with the carrier solution alone; mitotic figures are detectable (arrows); single plane. **B,** Melanoma cells in a brain metastasis of a mouse 11 days after start of treatment with GNE-317, with extensive abnormalities of nuclear morphology indicative of apoptosis (arrowheads); single plane. **C,** Nuclear changes (arrowheads) in a GDC-0980–treated permeable metastasis 3 days after start of treatment; single plane. **D,** Distances of nuclei with therapy-induced apoptotic changes from the nearest blood vessel (nonpermeable, GNE-317–treated metastasis 4 days after start of treatment), as detectable in the 3D-image stack. Arrow 1, distance to an apoptotic event measured from the nearest blood vessel; arrow 2, distance of the tumor cell nucleus that is most distant from this blood vessel, but not nearer to another blood vessel. By dividing these two values (1 divided by 2), the "blood vessel proximity index" for apoptotic events was calculated; right side, quantifications of this index for three experiment groups ($n = 12$ blood vessels per condition; $P > 0.05$; ANOVA). The red dotted line marks a blood vessel proximity index of "0.5," which would represent a situation where therapy-induced changes are equally seen in tumor cells near to and far from perfused microvessels in the brain. All images were acquired by *in vivo* MPLSM; 3D reconstruction of a *z*-stack of 12 μm (D); scale bars, 15 μm.

relevance. In consequence, this supports a "gatekeeper" function of the BBB for CNS drug penetration. Second, the perivascular niche itself seems to provide specific cues for survival and resistance in brain metastasis, which we have proposed before for brain-metastatic non–small cell lung cancer (NSCLC) and melanoma cell lines (17, 29).

The results of this study suggest that the PAM pathway might be a promising target to prevent and/or treat brain metastases. This is particularly interesting in the light of earlier studies that point toward a specific importance of the PAM pathway for the brain metastatic process. PI3K was found to be among a couple of genes that were specifically altered in brain metastases of various tumor entities when compared with the primary tumor of individual patients (30), confirming previous reports that found specific alterations of the PAM pathway in melanoma (31) and non–small lung cancer (32) brain metastases. Furthermore, PTEN loss (which leads to PAM pathway activation) was associated with shorter time to brain metastasis, but not lung, liver, or bone metastasis in stage IIIB/C melanoma (33). PTEN loss was also enriched in brain metastases in breast cancer (34, 35). In accordance with this, in a preclinical model of HER2-positive breast cancer, a brain-permeable PI3K inhibitor significantly increased the numbers of mice that were brain-metastasis free at the end of the experiment (36). Likewise, in another animal model of triple-negative breast cancer, the mTOR inhibitor temsirolimus reduced brain micro- and macrometastases when given with a low (but not a high) dose in monotherapy (37). Finally, it was recently confirmed that PI3K pathway inhibition demonstrates particularly good efficacy against brain metastatic melanoma cells (38).

The high variability of BBB permeability found in our study is in line with previous reports. In brain tumor clinical specimens, highly variable tumor levels have been found for different therapeutic agents (39). Likewise, a preclinical study found a highly variable uptake of doxorubicin and paclitaxel in different metastases from the same breast cancer cell line, so that cytotoxic concentrations were reached in only 10% of the most permeable metastases (7). In accordance with that, it is widely assumed that classical chemotherapies with proven activity on systemic metastases of many cancers have very limited, if any, activity on brain metastases (40), probably with the exception of the primary chemotherapy of lung cancer brain metastases (41). In contrast, many of the targeted small-molecule inhibitors do show a reasonable activity in brain metastases (42), including the BRAF inhibitor dabrafenib in melanoma (43). It remained unclear, however, which stages of the brain metastatic cascade can effectively be reached, particularly whether asymptomatic micrometastases, which are often protected behind an intact BBB, can effectively be reached. This is particularly relevant for the newer concept of brain metastasis prevention in patients who are currently brain-metastasis free but at high risk of developing them (2, 44, 45). In these patients, single tumor cells (or small groups of them) that have already metastasized to the brain but are residing behind an intact BBB need to be targeted to achieve maximum preventive efficacy. The fact that under GNE-317 treatment, only those micrometastases with an intact BBB shrank (and not just reduced their growth speed) might indicate that preventive regimens targeting single tumor cells or micrometastases could be more effective than the therapy for established macrometastases at later stages. Finally, the results of our study demonstrate that it is worthwhile to spend effort on improving the BBB penetration of drugs. Here, a rational chemical modification of an established, non-brain–permeable inhibitor was performed to improve physicochemical properties and reduce efflux by drug transporters expressed at the BBB, resulting in the brain-penetrant compound GNE-317 (14, 15).

A limitation of the study is the use of one melanoma cell line only. Our major aim was rather a principle clarification of the BBB function for brain metastasis biology and therapy. It is likely that other cell lines and tumor types with higher or lower sensitivity to PAM pathway interference in the brain may show different overall effects on permeable and nonpermeable brain metastases.

In conclusion, this study provides the direct visualization of how increased BBB permeability is associated with increased brain tumor growth, and how decreased BBB permeability hinders effective treatment of those brain metastasis cells that are hidden behind an intact BBB. Current data link the limited response to standard chemotherapy and subsequent dismal prognosis that is seen in some brain tumor subtypes to their particularly low BBB drug permeability (46). Together, it becomes evident that pharmacologic strategies that aim to increase drug penetration of the intact BBB bear the promise of a more positive impact on treatment responses of primary and metastatic brain tumors.

Disclosure of Potential Conflicts of Interest

L. Salphati has ownership interest (including patents) in Roche. H.S. Phillips is a consultant/advisory board member for Genentech/Roche. F. Winkler reports receiving commercial research grants from Boehringer, Genentech, and Roche. No potential conflicts of interest were disclosed by the other authors.

Authors' Contributions

Conception and design: M. Osswald, A.S. Berghoff, L. Salphati, J.J. Wallin, H.S. Phillips, W. Wick, F. Winkler

Development of methodology: M. Osswald, Y. Liao, M. Gömmel, A.S. Berghoff, F. Winkler

Acquisition of data (provided animals, acquired and managed patients, provided facilities, etc.): M. Osswald, J. Blaes, Y. Liao, A.S. Berghoff

Analysis and interpretation of data (e.g., statistical analysis, biostatistics, computational analysis): M. Osswald, J. Blaes, G. Solecki, A.S. Berghoff, L. Salphati, W. Wick, F. Winkler

Writing, review, and/or revision of the manuscript: M. Osswald, J. Blaes, Y. Liao, A.S. Berghoff, L. Salphati, J.J. Wallin, H.S. Phillips, W. Wick, F. Winkler

Administrative, technical, or material support (i.e., reporting or organizing data, constructing databases): M. Osswald, Y. Liao, M. Gömmel, A.S. Berghoff, F. Winkler

Study supervision: F. Winkler

Acknowledgments

We thank Petra Rübmann for technical assistance and Louisa von Baumgarten for help with the establishment of different techniques.

Grant Support

This work was supported by a research grant from Genentech, Inc. (to F. Winkler) and by grants from the German Research Foundation (DFG; WI 1930/5-1; to F. Winkler and Major Equipment Grant INST 114089/26-1 FUGG; to F. Winkler and W. Wick).

The costs of publication of this article were defrayed in part by the payment of page charges. This article must therefore be hereby marked *advertisement* in accordance with 18 U.S.C. Section 1734 solely to indicate this fact.

Received June 1, 2016; revised July 22, 2016; accepted July 28, 2016; published OnlineFirst August 12, 2016.

References

1. Gibney GT, Forsyth PA, Sondak VK. Melanoma in the brain: biology and therapeutic options. Melanoma Res 2012;22:177–83.
2. Steeg PS, Camphausen KA, Smith QR. Brain metastases as preventive and therapeutic targets. Nat Rev Cancer 2011;11:352–63.
3. Palmieri D, Chambers AF, Felding-Habermann B, Huang S, Steeg PS. The biology of metastasis to a sanctuary site. Clin Cancer Res 2007;13:1656–62.
4. Gerstner ER, Fine RL. Increased permeability of the blood-brain barrier to chemotherapy in metastatic brain tumors: establishing a treatment paradigm. J Clin Oncol 2007;25:2306–12.
5. Fortin D.The blood–brain barrier: its influence in the treatment of brain tumors metastases. Curr Cancer Drug Targets 2012;12:247–59.
6. Blecharz KG, Colla R, Rohde V, Vajkoczy P. Control of the blood-brain barrier function in cancer cell metastasis. Biol Cell 2015;107:342–71.
7. Lockman PR, Mittapalli RK, Taskar KS, Rudraraju V, Gril B, Bohn KA, et al. Heterogeneous blood-tumor barrier permeability determines drug efficacy in experimental brain metastases of breast cancer. Clin Cancer Res 2010;16:5664–78.
8. Morikawa A, Peereboom DM, Thorsheim HR, Samala R, Balyan R, Murphy CG, et al. Capecitabine and lapatinib uptake in surgically resected brain metastases from metastatic breast cancer patients: a prospective study. Neuro Oncol 2015;17:289–95.
9. Daneman R.The blood–brain barrier in health and disease. Ann Neurol 2012;72:648–72.
10. Weidle UH, Niewohner J, Tiefenthaler G. The blood–brain barrier challenge for the treatment of brain cancer, secondary brain metastases, and neurological diseases. Cancer Genomics Proteomics 2015;12:167–77.
11. Rodon J, Dienstmann R, Serra V, Tabernero J. Development of PI3K inhibitors: lessons learned from early clinical trials. Nat Rev Clin Oncol 2013;10:143–53.
12. Kwong LN, Davies MA. Navigating the therapeutic complexity of PI3K pathway inhibition in melanoma. Clin Cancer Res 2013;19:5310–9.
13. Elkabets M, Vora S, Juric D, Morse N, Mino-Kenudson M, Muranen T, et al. mTORC1 inhibition is required for sensitivity to PI3K p110alpha inhibitors in PIK3CA-mutant breast cancer. Sci Transl Med 2013;5:196ra99.
14. Salphati L, Heffron TP, Alicke B, Nishimura M, Barck K, Carano RA, et al. Targeting the PI3K pathway in the brain–efficacy of a PI3K inhibitor optimized to cross the blood–brain barrier. Clin Cancer Res 2012;18:6239–48.
15. Salphati L, Shahidi-Latham S, Quiason C, Barck K, Nishimura M, Alicke B, et al. Distribution of the phosphatidylinositol 3-kinase inhibitors pictilisib (GDC-0941) and GNE-317 in U87 and GS2 intracranial glioblastoma models-assessment by matrix-assisted laser desorption ionization imaging. Drug Metab Dispos 2014;42:1110–6.
16. Salphati L, Pang J, Plise EG, Lee LB, Olivero AG, Prior WW, et al. Preclinical assessment of the absorption and disposition of the phosphatidylinositol 3-kinase/mammalian target of rapamycin inhibitor GDC-0980 and prediction of its pharmacokinetics and efficacy in human. Drug Metab Dispos 2012;40:1785–96.
17. Kienast Y, von Baumgarten L, Fuhrmann M, Klinkert WE, Goldbrunner R, Herms J, et al. Real-time imaging reveals the single steps of brain metastasis formation. Nat Med 2010;16:116–22.
18. Weiler M, Blaes J, Pusch S, Sahm F, Czabanka M, Luger S, et al. mTOR target NDRG1 confers MGMT-dependent resistance to alkylating chemotherapy. Proc Natl Acad Sci U S A 2014;111:409–14.
19. Kessler T, Sahm F, Blaes J, Osswald M, Rubmann P, Milford D, et al. Glioma cell VEGFR-2 confers resistance to chemotherapeutic and antiangiogenic treatments in PTEN-deficient glioblastoma. Oncotarget 2015;6:31050–68.
20. Opitz CA, Litzenburger UM, Sahm F, Ott M, Tritschler I, Trump S, et al. An endogenous tumour-promoting ligand of the human aryl hydrocarbon receptor. Nature 2011;478:197–203.
21. Osswald M, Jung E, Sahm F, Solecki G, Venkataramani V, Blaes J, et al. Brain tumour cells interconnect to a functional and resistant network. Nature 2015;528:93–8.
22. Kaya M, Ahishali B. Assessment of permeability in barrier type of endothelium in brain using tracers: Evans blue, sodium fluorescein, and horseradish peroxidase. Methods Mol Biol 2011;763:369–82.
23. Kerr JF, Wyllie AH, Currie AR. Apoptosis: a basic biological phenomenon with wide-ranging implications in tissue kinetics. Br J Cancer 1972;26:239–57.
24. Gaudino S, Di Lella GM, Russo R, Lo Russo VS, Piludu F, Quaglio FR, et al. Magnetic resonance imaging of solitary brain metastases: main findings of nonmorphological sequences. Radiol Med 2012;117:1225–41.

25. Fidler IJ, Yano S, Zhang RD, Fujimaki T, Bucana CD. The seed and soil hypothesis: vascularisation and brain metastases. Lancet Oncol 2002;3:53–7.
26. Percy DB, Ribot EJ, Chen Y, McFadden C, Simedrea C, Steeg PS, et al. *In vivo* characterization of changing blood-tumor barrier permeability in a mouse model of breast cancer metastasis: a complementary magnetic resonance imaging approach. Invest Radiol 2011;46:718–25.
27. Adkins CE, Mohammad AS, Terrell-Hall TB, Dolan EL, Shah N, Sechrest E, et al. Characterization of passive permeability at the blood-tumor barrier in five preclinical models of brain metastases of breast cancer. Clin Exp Metastasis 2016;33:373–83.
28. Zhang RD, Price JE, Fujimaki T, Bucana CD, Fidler IJ. Differential permeability of the blood-brain barrier in experimental brain metastases produced by human neoplasms implanted into nude mice. Am J Pathol 1992;141:1115–24.
29. Winkler F.The brain metastatic niche. J Mol Med 2015;93:1213–20.
30. Brastianos PK, Carter SL, Santagata S, Cahill DP, Taylor-Weiner A, Jones RT, et al. Genomic characterization of brain metastases reveals branched evolution and potential therapeutic targets. Cancer Discov 2015;5:1164–77.
31. Chen G, Chakravarti N, Aardalen K, Lazar AJ, Tetzlaff MT, Wubbenhorst B, et al. Molecular profiling of patient-matched brain and extracranial melanoma metastases implicates the PI3K pathway as a therapeutic target. Clin Cancer Res 2014;20:5537–46.
32. Li Q, Yang J, Yu Q, Wu H, Liu B, Xiong H, et al. Associations between single-nucleotide polymorphisms in the PI3K-PTEN-AKT-mTOR pathway and increased risk of brain metastasis in patients with non–small cell lung cancer. Clin Cancer Res 2013;19:6252–60.
33. Bucheit AD, Chen G, Siroy A, Tetzlaff M, Broaddus R, Milton D, et al. Complete loss of PTEN protein expression correlates with shorter time to brain metastasis and survival in stage IIIB/C melanoma patients with BRAFV600 mutations. Clin Cancer Res 2014;20:5527–36.
34. Hohensee I, Lamszus K, Riethdorf S, Meyer-Staeckling S, Glatzel M, Matschke J, et al. Frequent genetic alterations in EGFR- and HER2-driven pathways in breast cancer brain metastases. Am J Pathol 2013;183:83–95.
35. Wikman H, Lamszus K, Detels N, Uslar L, Wrage M, Benner C, et al. Relevance of PTEN loss in brain metastasis formation in breast cancer patients. Breast Cancer Res 2012;14:R49.
36. Nanni P, Nicoletti G, Palladini A, Croci S, Murgo A, Ianzano ML, et al. Multiorgan metastasis of human HER-2^{+} breast cancer in Rag2$^{-/-}$; Il2rg$^{-/-}$ mice and treatment with PI3K inhibitor. PLoS ONE 2012;7:e39626.
37. Zhao H, Cui K, Nie F, Wang L, Brandl MB, Jin G, et al. The effect of mTOR inhibition alone or combined with MEK inhibitors on brain metastasis: an *in vivo* analysis in triple-negative breast cancer models. Breast Cancer Res Treat 2012;131:425–36.
38. Niessner H, Schmitz J, Tabatabai G, Schmid A, Calaminus C, Sinnberg T, et al. PI3K pathway inhibition achieves potent antitumor activity in melanoma brain metastases *in vitro* and *in vivo*. Clin Cancer Res 2016 Jun 15. [Epub ahead of print].
39. Pitz MW, Desai A, Grossman SA, Blakeley JO. Tissue concentration of systemically administered antineoplastic agents in human brain tumors. J Neurooncol 2011;104:629–38.
40. Preusser M, Capper D, Ilhan-Mutlu A, Berghoff AS, Birner P, Bartsch R, et al. Brain metastases: pathobiology and emerging targeted therapies. Acta Neuropathol 2012;123:205–22.
41. Barlesi F, Gervais R, Lena H, Hureaux J, Berard H, Paillotin D, et al. Pemetrexed and cisplatin as first-line chemotherapy for advanced non-small-cell lung cancer (NSCLC) with asymptomatic inoperable brain metastases: a multicenter phase II trial (GFPC 07-01). Ann Oncol 2011;22:2466–70.
42. Ahluwalia MS, Winkler F. Targeted and immunotherapeutic approaches in brain metastases. Am Soc Clin Oncol Educ Book 2015;35:67–74.
43. Long GV, Trefzer U, Davies MA, Kefford RF, Ascierto PA, Chapman PB, et al. Dabrafenib in patients with Val600Glu or Val600Lys BRAF-mutant melanoma metastatic to the brain (BREAK-MB): a multicentre, open-label, phase 2 trial. Lancet Oncol 2012;13:1087–95.
44. Steeg PS. Perspective: the right trials. Nature 2012;485:S58–9.
45. Ilhan-Mutlu A, Osswald M, Liao Y, Goemmel M, Reck M, Miles D, et al. Bevacizumab prevents brain metastases formation in lung adenocarcinoma. Mol Cancer Ther 2016;15:702–10.
46. Phoenix TN, Patmore DM, Boop S, Boulos N, Jacus MO, Patel YT, et al. Medulloblastoma genotype dictates blood–brain barrier phenotype. Cancer Cell 2016;29:508–22.